Egypt. J. Chem. **Vol. 65,** No. 5 pp. 33 - 47 (2022)

Egyptian Journal of Chemistry

http://ejchem.journals.ekb.eg/

Polyacrylamide Grafted Electrospun Polyamide 6 Nanocomposite Fibers for Drug Delivery Application

Amira N Shehab-ElDin[a], Rokaya A. Sobh[a]*, Abdelgawad M. Rabie[b], Wael S. Mohamed[a], Hanaa E. Nasr[a]

[a]*Polymers & Pigments Department, National Research Centre, Dokki, Giza, Egypt.*

[b]*Chemistry Department, Faculty of Science, Ain Shams University, Cairo, Egypt.*

Abstract

PA6 nanofibers have gained increasing interest as a potential candidate for medical applications. In this work, tallow modified clay (TMC) was incorporated into PA6 electrospun nanofibers. The fabricated nanocomposite fiber was chemically modified through the grafting with polyacrylamide using potassium persulfate and sodium hydrogen sulfite as redox initiation system. The effects of temperature, initiator and monomer concentrations as well as reaction duration on the grafting reaction were studied. In addition, methylene bis acrylamide, as a crosslinker, was added to obtain crosslinked polyacrylamide hydrogel layer grafted to the nanofibers. Doxycycline hydrochloride as a potent broad spectrum antibiotic was loaded to the crosslinked polyacrylamide grafted material through the swelling diffusion method. The addition of tallow modified clay (TMC) into PA6 nanofibers dramatically influenced the morphology, thermal stability, and mechanical properties as confirmed from SEM, TGA, and mechanical testing. In addition, the grafted nanofibrous mat was characterized by FTIR, SEM, TGA and contact angle measurement. The crosslinked polyacrylamide grafted nanofibrous mat was assessed as a drug delivery vehicle for drug loading, drug release behaviour, and antimicrobial properties. The results showed that the loaded drug released fast in both phosphate buffer saline PBS (pH 7.4) and acetate buffer (pH 5.5) and initial burst release was observed in the first two hours. Furthermore, the antimicrobial evaluation of loaded grafted nanofibrous mat against *E. coli* and *S. aureus* confirmed the antimicrobial activity of loaded materials.

***Keywords*:** Tallow modified clay, electrospun nanofibers, polyacrylamide grafted nanofibers, drug delivery

1. Introduction

Polyamide 6 (PA6) is a synthetic semicrystalline polymer that has found several applications in diverse fields such as environmental remediation [1], textile fibers [2], automotive parts [3] and food packaging [4]. Recently, it has gained growing interest in biology and medical applications due to its biocompatibility (structural similarity to peptides due to presence of amide linkages), flexibility, mechanical strength and high resistance to chemicals and body fluids [5]. Incorporating nanofillers into polymer matrix produces polymer nanocomposites with improved physical properties such as enhanced thermal stability, mechanical strength and modulus even at low filler loading [6]. Clay minerals are the most widely used nanofillers to prepare polymer-based nanocomposites as they are available and of low cost and have a high surface area to volume ratio. However, pristine clays are highly hydrophilic making them incompatible with most polymeric matrices [7]. Thus, the successful development of polymer clay nanocomposites necessitates chemical modification of hydrophilic clay surface to change it into a more organophilic one [8]. Generally, quaternary alkylammonium or alkylphosphonium cationic surfactants are used in quantities excess to clay mineral cation exchange capacity (CEC) to preplace the hydrated interlayer cations (K^+, Na^+, Ca^2) through ion exchange reactions resulting in expansion of interlayer galleries, lowering the surface energy and improving the wetting properties with the polymer matrix [9]. Polymeric nanofibers have received a great deal of attention in recent years due to their outstanding characteristics: they possess

*Corresponding author e-mail: rokaya_aly@yahoo.com.
Receive Date: 04 February 2022, Revise Date: 19 February 2022, Accept Date: 20 February 2022
DOI: 10.21608/EJCHEM.2022.119754.5386
©2022 National Information and Documentation Center (NIDOC)

controllable porosity, superior surface flexibility, high surface area to volume ratio (can reach 10^3 times larger than microfibers), flexibility to design nanofibers with various compositions to tailor properties and function, and enhanc mechanical performance. Furthermore, they mimic the biophysical nature of the extracellular matrix [10]. All these features strongly nominate polymer nanofibers in a wide range of applications such as tissue engineering [11], enzyme immobilization [12], filtration [13], wound dressing [14] and drug delivery application [15]. Electrospinning has particularly received widespread attention for the fabrication of polymer nanofibers as it is a facile, efficient, cost-effective and adaptable polymer processing technique to fabricate fibres in the nano scale range [16]. Grafting is a well-established technique to modify synthetic fibers and films. It is intended to alleviate some drawbacks and / or to add new functionalities to improve the physicochemical properties, adsorption, pH sensitivity, swelling ability, and thermal and morphological features [17]. Several factors such as initiator system, monomer type, temperature, reaction time, reaction environment (vacuum, inert atmosphere, atmospheric conditions), and addition of crosslinker agents and their concentration control the grafting reaction [18]. Several polymers have been selected for surface modification to conjugate drugs, enhance their loading capability, and control their release profile. Polyethyleneimine, which bears numerous primary and secondary amine functional groups in its structure; has been employed to develop high-performance drug delivery systems. Other polymers such as polymethacrylic acid and polyacrylamide as well are considered important materials for surface modification as drug delivery systems due to their outstanding swelling ability, and biocompatibility [19, 20]. In current work, PA6/TMC nanocomposite fibrous mat was chemically modified through grafting copolymerization of acrylamide, using a redox initiation system consisting of potassium persulfate (oxidizing agent) and sodium hydrogen sulfite (reducing agent) in a 1:2 molar ratio respectively. N, N – methylene – bis – acrylamide was used as a crosslinker to obtain a hydrogel graft layer of crosslinked polyacrylamide. The factors affect the grafting process as monomer and initiator concentrations, temperature, time of reaction, and addition of crosslinker were also studied. The prepared crosslinked polyacrylamide grafted nanofibrous mat was further investigated as a drug carrier for doxycycline hydrochloride. Drug release behavior was investigated in PBS (pH 7.4) and acetate buffer (pH 5.5). On the other hand, the antimicrobial evaluation of the loaded material was performed against *E.coli*, and *S. aureus* as examples of gram-negative and gram-positive bacteria respectively.

2. Materials and methods

2.1. Materials

Nanoclay (hydrophilic bentonite), dihydrogenated tallow dimethyl ammonium chloride (Arquad® 2HT-75), and phosphate buffered saline tablets (PBS) were purchased from Sigma Aldrich. Polyamide 6 (low molecular weight), N, N – methylene – bis – acrylamide (assay ≥ 98%), and sodium acetate trihydrate were obtained from Fluka. Doxycycline hydrochloride (F.W. 480.9) was bought from Fisher Scientific. Acrylamide (minimum assay 98.5%), potassium persulphate ($K_2S_2O_8$, M. Wt. 270.31, minimum assay 98%), and sodium hydrogen sulphite ($NaHSO_3$ M. Wt. 104.07) were obtained from s. d. fine – chem limited. Formic acid (85% v/v) from El-Nasr Pharmaceutical Chemical Co., Egypt and glacial acetic acid was obtained from Alpha chemika, India.

2.2. Preparation of tallow modified clay (TMC)

Tallow modified clay (TMC) was obtained according to previous work **[21]**. In brief, 2.5 g of pristine clay was dispersed in 250 ml of distilled water at 80℃ using a magnetic stirrer for 1h. In another 50 ml distilled water at 80 ℃, the required weight of the tallow (ranging from 0.5:1 to 2:1 T/clay w/w ratio) was dissolved separately. Then, the tallow solution was mixed drop wise with the clay dispersion and stirred overnight at room temperature. The obtained TMC was filtered and washed with 250 ml distilled water at 80 ℃ three times to get rid of any excess unreacted tallow, then freeze dried and stored for further use**.**

2.3. Fabrication of nanofibrous mats

The neat PA6 nanofibers in formic acid were prepared from (35% w/v) polymer solution. To fabricate PA6/TMC nanocomposite nanofibers, TMC was added to PA6 solution at various loadings ranging from 0.5 to 1% based on the polymer dry weight and stirred overnight and bath sonicated (Ultrasonic bath MTI, model UD50SH-2LQ, 50W) for 1h to obtain homogenous solution. 1ml of this solution was placed in a syringe fitted with 20 G blunt needle tip and electrospun at ambient condition, applied 20 KV, 10 cm needle to collector distance and 0.25 ml/h flow rate **[22].**

2.4. Modification of PA6/TMC nanocomposite fibrous mat

PA6/TMC nanocomposite nanofibers were chemically modified through graft polymerization of acrylamide **[23]**, a hydrophilic monomer using potassium persulfate/sodium hydrogen sulfite redox initiation system at molar ratio of 1:2. Sample of 1.5 × 1.5 cm and 0.35 mm thickness of the nanofibrous mat was placed in 50 ml distilled water containing the desired quantity of monomer and crosslinker (in case of preparing crosslinked polyacrylamide grafted material) in a round bottom flask fitted with a condenser at a preset temperature water bath. Then, the activator was added followed by the initiator to initiate the polymerization reaction under full exposure to atmospheric oxygen and the contents of the flask were shaken occasionally. After the specific period, the sample was removed from the reaction medium and washed thoroughly with hot distilled water several times to get rid of the homopolymer then dried at 40 ℃ in an oven until a constant weight.

The grafting percentage was estimated according to equation **(1) [24]**:

$$\mathbf{G\ \% = [(W_1 - W_0)/ W_0] \times 100} \qquad \mathbf{(1)}$$

(W_0) is the initial weight of the dry sample and **(W_1)** is its weight after grafting.

- **Swelling behaviour**

Swelling of crosslinked polyacrylamide grafted nanofibrous mat was carried out in 25 ml of PBS (pH 7.4) at 37 ℃. The weight of dry grafted sample was estimated then placed in a tea bag and soaked in the swelling medium **[25]**. At specific time intervals, the tea bag was taken out from the swelling medium, drained, and wiped with tissue paper to remove excess water. The weight of swollen hydrogel sample was estimated and the swelling ratio was calculated from equation **(2) [26]**

$$\text{Swelling ratio} = (W_t - W_0) / W_0 \times 100 \qquad \mathbf{(2)}$$

(W_0) is the initial weight of the dry sample, and **(W_t)** is the weight of swollen sample at estimated time points.

2.5. Drug loading

Doxycycline hydrochloride was loaded to crosslinked polyacrylamide grafted PA6/TMC nanofibrous mat by swelling diffusion method **[19, 27]**. The grafted 1.5 × 1.5 cm nanofibrous mat sample was immersed in a glass vial containing 10 ml of doxycycline hydrochloride solution (10 mg/ml) at pH 4, and pH 6 for six hours to complete the drug loading process. Then the sample was removed from the drug solution and freeze dried.

- **Drug content**

A drug-loaded sample was immersed in 30 ml of PBS buffer (pH 7.4) for 24 hours to elute the drug completely. The mass of drug released in the medium was quantified by UV spectrophotometer (Jasco V-630, Japan) at 273 nm using the constructed standard calibration curve.

2.6. In vitro drug release studies

The drug release studies from crosslinked polyacrylamide grafted PA6/TMC nanofibrous mat were performed in phosphate buffer saline (PBS) at (pH 7.4), and acetate buffer (pH 5.5) using cellulose dialysis bag technique according to **[28, 29]**. The dialysis tube (14 kD MW cutoff, Sigma Aldrich) was first soaked and equilibrated in amount of the release medium for several hours, and then the drug loaded mat was placed in the tube and immersed in 25ml of buffer solution at 37ºC ±1. At the specific time intervals 2ml of the release medium was collected in Eppindorff tubes and compensated for equal amounts of preheated fresh release medium to maintain the sinking properties. The samples with high concentrations were diluted with suitable and known dilution factors and the mass of the drug was quantified spectrophotometrically at 273 nm for PBS and 275 nm for acetate buffer.

2.7. Antimicrobial evaluation

The antimicrobial properties were evaluated by estimating the inhibition zones expressed in mm using the disk diffusion method. Nutrient agar plates containing 20 ml of sterile medium were prepared and inoculated with 25µl of tested microorganisms suspensions including approximately 0.5 Mc Farland standard (1.5×10^8 CFU /mL) **[30]**.

The antimicrobial activity of drug loaded crosslinked polyacrylamide grafted PA6/TMC nanofibers samples was investigated against two pathogenic bacteria; *Escherichia coli* (ATCC 25922), and *Staphyllococcus aureus* (ATCC 6538). The drug was loaded to the tested samples and estimated experimentally by UV spectrophotometer using standard calibration curve, and blank sterile susceptibility tested discs (Himedia, India, Lot 0000409749, Exp 10/2022). They were impregnated with the equivalent mass of free doxycycline hydrochloride drug dissolved in water (purified water for reconstitution of dry powder from Pharma pack Pharmaceutical Industries, Egypt) and applied as the positive control. In addition, blank grafted PA6/TMC nanofiberous mat samples were tested as negative controls. All samples were put on the plates and incubated at 37 ℃ for 24h **[31]**. Inhibition Zones (clear zones around the applied samples) expressed in mm were measured by calipers and imageJ® software

2.8. Characterization methods

X- ray diffraction analyses (XRD) of unmodified clay, TMC1:1, neat PA6 nanofibers, and PA6/TMC nanocomposite nanofibers containing 1% TMC were performed using (Model: X'PERT – PRO – PAN analytical – Netherland) operating at 30mA, and 40KV. X-ray source was CuKα (λ=1.5406) and the samples were scanned between 0.5° and 10° (2Θ) with a step size of 0.02° and 10°. Moreover, the structural changes for the investigated compounds were estimated by ATR FT-IR (Vertex 80V Bruker 4 cm^{-1} resolution) in the range from 4000-400 cm^{-1}.
Thermal stability of the prepared compounds was investigated using (sdtQ 600 TA, USA) instrument. A sample mass of about 3-5 mg was heated under nitrogen at the rate of 10 ℃/min in the range from 50℃ to 600 ℃.

The surface charge of both pristine clay and TMC 1:1 was estimated by measuring zeta potential values in 0.05% aqueous dispersion at 25 ℃ using (Malvern Zeta Sizer – Nano-series, UK).

The viscosity measurements were carried out using Brookfield viscometer (model DV-III Ultra, UK), spindle 21 at 10 rpm under ambient temperature.

A conductivity meter (HC3010, Trans instruments) was used to estimate the conductivity values for neat PA6 solution, and PA6/TMC nanocomposite solutions contain various loadings of TMC 1:1.

The morphology of unmodified clay, TMC1:1, neat PA6 nanofibers, PA6/TMC nanocomposite nanofibers, and polyacrylamide grafted PA6/TMC nanofibers (76% grafting ratio) were investigated by high resolution scanning electron microscopy (Quanta FEG250 with field emission gun, FEI, Nertherlands). Small samples of dried materials were applied to sticky carbon tape and sputter-coated for 3 minutes to introduce a thin layer of gold. Images with various magnifications were taken, and a representative one was considered. The dispersion of clay into PA6 nanofibers was investigated using (HR-TEM, JEOL, JEM-2100, Japan). TEM analysis was carried out on previously deposited fibers on 200 mesh carbon coated copper grid.

The mechanical properties of neat PA6 nanofibers, and PA6/TMC nanocomposite nanofibers with 1% TMC1:1 were tested using (Instron 34SC-5) at the speed of 10 mm/min at room temperature. The tested materials were cut into rectangular specimens of dimensions (60, 10, and 0.15) mm. Three specimens were tested and values were averaged.

Water contact angles for electrospun PA6/TMC nanocomposite nanofibers and polyacrylamide grafted PA6/TMC nanofibers (76% grafting ratio) were measured using (OCA I5EC contact angle model produced by the company of Data Physics Instrument Gmbh). A deionized water drop of 0.5 µl was applied on the surface of electrospun materials at room condition and allowed to stand for about 10s before capturing images. The angle between the nanofibrous mat – water interface and the water – air interface was measured. About 3 measurements on different locations on the sample were performed and averaged.

3. Results and discussion

3.1. Clay modification

The hydrophilic bentonite clay was modified by dihydrogenated tallow dimethyl ammonium chloride as organic quaternary ammonium surfactant through cation exchange reaction in which, the hydrophilic cations such as (Na^+ and Ca^{2+}) present in clay interlayer galleries are exchanged by the organic quaternary ammonium salt to result in the expansion of basal spacing of clay. This modification transforms natural hydrophilic clay to more organophilic material and consequently improves its compatibility and dispersiability with polymer matrix and organoclays have been extensively used as fillers in polymer matrix formulations **[33].**

Herein, pristine clay was modified with various ratios of the organomodifier and the effect of modifier content on basal spacing, structure, thermal stability, surface charge and morphology was investigated with XRD, FT-IR, TGA, Zeta potential and SEM, respectively.

- **X-ray diffraction (XRD)**

Successful intercalation of the long alkyl chain quaternary ammonium salt (tallow) into clay interlayer was confirmed from the results of XRD analysis as shown in **Table (1)** and **Fig. (1).** It was noticed that there was a shift towards lower 2Θ values and a gradual increase in basal spacing of clay as the loading of organomodifier increased. The basal spacing of unmodified clay was 14.32 and increased to 39.35 for TMC at modifier/clay 1:1 (w/w) ratio, and then with further organomodifier content increment, the basal spacing almost reached a steady state **[32]**.

Table 1: Effect of organomodifier loading on basal spacing of clay

Sample Type	T/clay (w/w) ratio	D-spacing
Pristine clay	0:1	14.32
TMC	0.5:1	34.46
	1:1	39.35
	1.5:1	40.47
	2:1	41.96

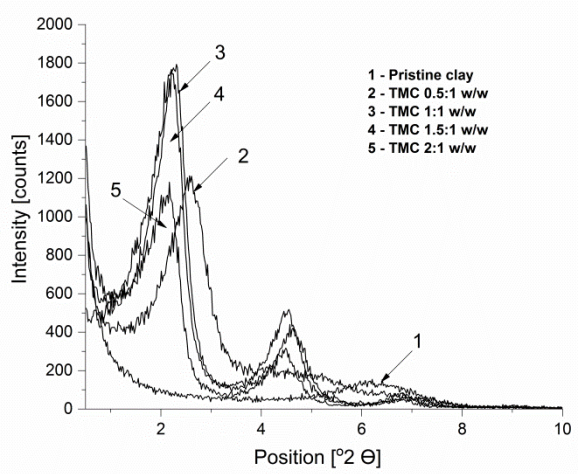

Figure (1): X-ray diffraction analysis of pristine clay, and TMC with various modifier loading

- **Fourier transform infrared spectroscopy (FT-IR)**

The structural changes of pristine clay and TMC1:1 are presented in **Fig. (2),** where, the peaks observed at 3612-3616 cm^{-1} are features of O−H stretching, while the other peaks appeared at 1633-1645 cm^{-1} are due to O−H bending vibrations.

The appearance of strong peaks at 2917 cm^{-1} and 2850 cm^{-1} after clay modification are attributed to CH_2 asymmetric and symmetric vibrations respectively, and the peak at 1467 cm^{-1} is due to C−N functionality. These peaks were completely absent in the spectra of pristine clay, which confirmed the successful modification of clay with Tallow **[32, 8]**.

- **Thermal gravimetric analysis (TGA)**

The thermal analyses data of pristine clay and TMC were studied from 50 to 600 ℃. TGA gives perspective about the thermal stability and degradation of organomodified clay. The TGA results and thermograms of both pristine and TMC 1:1 are shown in **Table (2)** and **Fig. (3).** It can be seen that unmodified clay showed prolonged thermal stability as it went through several steps; the first stage of mass loss was observed up to 102 ℃ owing to moist desorption, followed by dehydration of interlayer cations and dehydroxylation of clay respectively **[8].** The presence of intercalated organic surfactant increased the degradation steps. It is noticed that, the onset decomposition temperature of TMC was higher than pristine clay due to the formation of new bonds between the organomodifier present in interlayer galleries and clay. However, TMC exhibited significant mass loss between 270 ℃ and 450 ℃, which was much higher than pristine clay due to the destruction of bonds between the organomodifier molecules and decomposition of the intercalated modifier. The obtained results are consistent with the previously reported data **[8, 33].**

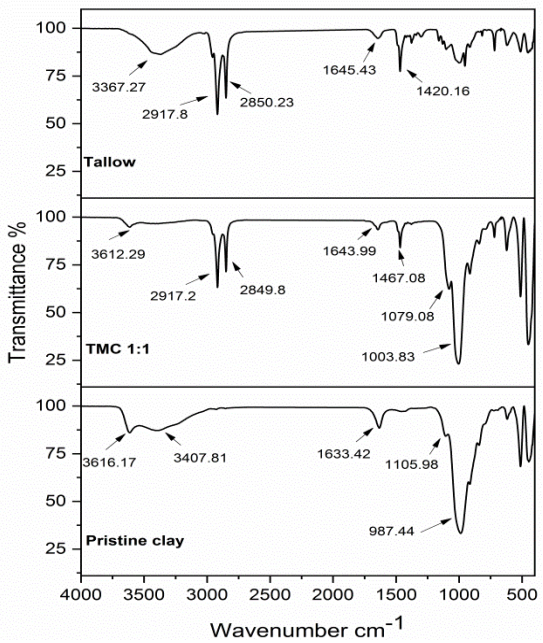

Figure (2): FT-IR spectra for unmodified clay, organomodifier (Tallow) and TMC 1:1 w/w ratio

Table (2): TGA results for pristine clay and TMC 1:1 (T/clay w/w ratio)

Sample type	Decomposition Temperature (℃)						
	T 10%	T 15%	T 20%	T 25%	T 30%	T 50%	T 60%
Pristine clay	102	190.8	416.7	560	-	-	-
TMC 1:1	253	274	291	305	318	387	446

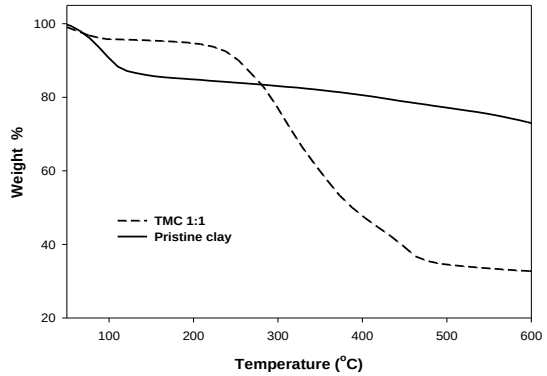

Figure (3): TGA curves for pristine clay and TMC 1:1

- **Surface charge**

The surface charge of clay is of great importance as it determines clay – clay and/or clay – ions interactions **[34]**. Zeta potential (electrostatic potential) measures the surface charge density by estimating the repose of a sample dispersed in a liquid under application of electric field.

The zeta potential value for pristine clay was measured as (-30 mV) owing to the structural charge resulting from isomorphic substitution in octahedral sheets. After modification of clay with tallow (TMC 1:1), the surface charge measured (-17 mV) as proportion of the cationic surfactant was adsorbed on clay surface through electrostatic interaction **[35]**.

- **Scanning electron microscopy (SEM)**

SEM images indicated significant morphological changes between pristine clay and TMC1:1, as observed from **Fig. (4).** Pristine clay appeared as large aggregated particles that indicates poorly dispersed clay particles. After modification, TMC1:1 showed less aggregation and packing density of layers hence well dispersed clay particles **[36]**.

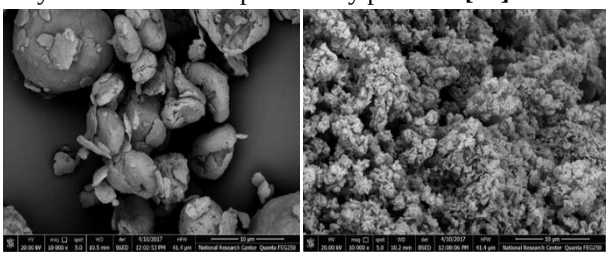

a **b**

Figure (4): SEM images of (a) pristine clay and (b) TMC 1:1 w/w ratio

3.2. PA6 and / PA6/TMC electrospun nanofibers production:

PA6 solution in formic acid at concentration of 35% w/v was prepared. Further, TMC1:1 was incorporated into PA6 solution with various ratios producing PA6/TMC nanocomposite solutions containing various loadings of TMC1:1 ranging from (0.5 - 1% w/w). The effect of TMC loading on the physical properties of PA6 solution was characterized in terms of viscosity and conductivity of PA6 and PA6/TMC nanocomposite solutions that are represented in **Table (3)**. It was observed that the addition of TMC to PA6 solution caused an initial decrease in both viscosity and conductivity values of PA6 solution at the lowest concentration of TMC (0.5% w/w). Then viscosity and conductivity values increased gradually with TMC increase **[22].**

- **Fiber morphology**

SEM images of neat PA6 nanofibers and PA6/TMC nanocomposite nanofibers containing various loadings of TMC1:1 ranging from (0.5 - 1% w/w) are presented in **Fig. (5).** It can be observed that, electrospinning of neat PA6 solution at concentration of 35% w/v produced homogenous and beads free nanofibers with few cracks and average diameter of 74 ± 4.42 nm. Furthermore, it confirmed that the polymer solution concentration was sufficient to enhance chain entanglements and to stabilize the polymer jet throughout the electrospinning process **[22, 37]**. The addition of various contents of TMC1:1 (e.g., 0.5, 0.75, 1% w/w ratio) into electrospinning of PA6 solution had a dramatic effect on morphology, as shown in **Fig. (5)**.

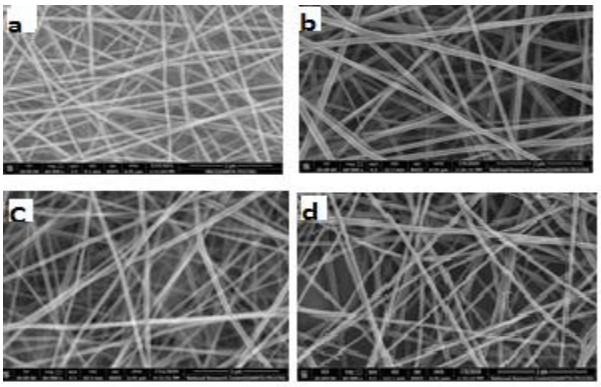

Figure (5): SEM images of electrospun nanofibers for (a) neat PA6 35% w/v, (b) PA6/TMC 0.5% w/w, (c) PA6/TMC 0.75% w/w and (d) PA6/TMC 1% w/w

Smooth and homogeneous fibers with increased the average diameter as 105 ± 12.53 nm were obtained by adding 0.5% w/w of TMC. It was also observed that, the average diameter of PA6/TMC nanocomposite nanofibers steadily decreased with further increasing TMC loading; the addition of 0.75 % w/w of TMC decreased the fibers average diameter to 90.1 ± 13.56 nm and further increased TMC content to 1% w/w, nanofibers with average diameter of 78.5 ± 3.92 nm were obtained. It could be attributed to the presence of positively charged quaternary ammonium salt (organomodifier) between clay interlayers that increased the charge and conductivity of polymer solution as summarized in table (3) and resulted in improved morphology **[38]**.

Table (3): Effect of TMC loading on physical properties of PA6 solution and the corresponding average diameter of obtained fibers Values are presented as mean ± S.D.

Sample type	Concentration w/v	TMC content w/w ratio	Viscosity cp	Conductivity µS	Average diameter nm.
Neat PA6	35%	-	1750 ± 13.23	3.88 ± 0.05	74.2 ± 4.42
PA6/TMC	35%	0.5%	1730 ± 9.17	3.5 ± 0.04	105 ± 12.53
		0.75%	1760 ± 16.82	3.58 ± 0.03	90.1 ± 13.56
		1%	1795 ± 19.08	3.66 ± 0.04	78.5 ± 3.92

- **Thermal gravimetric analysis (TGA)**

TGA thermograms for neat PA6 nanofibers and PA6/TMC nanocomposite nanofibers containing 1% TMC in the range from 50 - 600℃ are represented in **Fig. (6-a).** It was observed that the nanocomposite nanofibers showed higher decomposition temperatures compared to neat PA6 nanofibers **[39, 40]**. The temperatures at 10% weight loss were 410 ℃ for nanocomposite nanofibers and 382.64 ℃ for neat PA6 as summarized in table (4). Furthermore,

the mass loss rate in case of nanocomposite nanofibers was slower than that for neat PA6, and the residual mass for PA6/TMC nanofibers was about 17.8 % compared to only 4.38 % for neat PA6 at 600℃ **[41].**

Table (4): TGA results for neat PA6 nanofibers and PA6/TMC nanocomposite nanofibers with 1% TMC

Sample type	Decomposition Temperature (℃)					
	T 10%	T 20%	T 30%	T 50%	T 70%	T 80%
Neat PA6 nanofibers	382.64	411.84	423.27	435.98	445.38	450.2
PA6/TMC nanofibers	410	422	430	441.8	454	464

- **Mechanical properties**

Mechanical properties of nanocomposite nanofibers are greatly influenced by the extent of nanofiller dispersion, fiber size and orientation **[38, 42]**. Stress – strain curves for both neat PA6 nanofibers prepared at a concentration of 35% w/v, and PA6/TMC nanocomposite nanofibers with 1% TMC are shown in **Fig. (6- b).** Young's modulus, tensile stress at maximum force, and tensile strain at break values are summarized in table (5). The Young's modulus increased after adding 1% TMC into PA6 nanofibers by about 12.8% improvement indicating enhanced stiffness owing to the reinforcing effect of organoclay **[42]**. In the same manner, the tensile stress, and tensile strain were considerably enhanced after incorporation of 1% TMC from 4 ± 0.24 to 6.08 ± 0.77 [MPa] and from 18.03 ± 0.09 to 22.65 ± 1.93[%] respectively **[43].** Enhancement of mechanical properties of PA6/TMC nanocomposite nanofibers containing 1% organoclay provides evidence of the organoclay's good dispersion within the PA6 matrix. Consequently, when the nanocomposite nanofiber is under the impact, nanoclay is difficult to detach from the polymer matrix, efficiently resist the applied force and transfers it to the surrounding matrix **[44]**.

Table (5): Mechanical properties of neat PA6 and PA6/TMC nanocomposite nanofibers containing 1% TMC. Data are presented as mean ± S.D.

Sample type	Young's modulus [MPa]	Tensile stress at maximum force [MPa]	Tensile strain at break [%]
Neat PA6	32.63 ± 3.35	4 ± 0.24	18.03 ± 0.09
PA6/TMC	36.8 ± 6.61	6.08 ±0.77	22.65 ± 1.93

- **X-Ray diffraction analysis (XRD)**

Small-angle X-ray diffraction (SAXRD) was carried out to examine the extent of organoclay dispersion in polymer matrix. The XRD patterns for TMC1:1, neat PA6 nanofibers, and PA6/TMC nanocomposite nanofibers with 1% TMC are illustrated in **Fig. (6- c).** The XRD pattern of TMC1:1 showed a reflection peak at 2Θ = 2.24º corresponding to d-spacing of 39.35 Å. While neat PA6 nanofibers did not show any observable reflection peaks in SAXRD region. By adding 1% of TMC into PA6, a broad diffraction peak at 2Θ = 2.28º was observed, verifying formation of intercalated nanostructure **[43]**.

- **Transmission electron microscope (TEM)**

TEM is a helpful tool to investigate further the degree of nanofiller dispersion in the polymer matrix. **Fig. (6- d)** shows TEM image for PA6/TMC1:1 nanocomposite nanofibers with 1% TMC1:1. The presence of dark areas distributed throughout the fiber gives speculation about the entry of PA6 polymer into clay interlayer and formation of intercalated structures, which confirmed by combining the results obtained from SEM, XRD, and TEM **[41, 43]**.

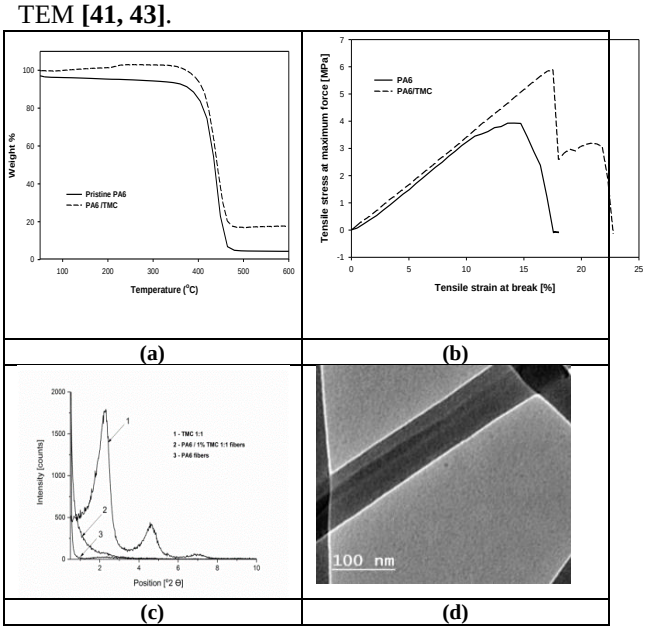

Figure (6): (a) TGA curves and **(b)** Stress – strain curves for neat PA6 nanofibers and PA6/TMC nanocomposite nanofibers with 1% TMC, **(c)** XRD patterns of TMC1:1, neat PA6 nanofibers, and PA6/TMC nanocomposite nanofibers with 1% TMC. **(d)** TEM images of PA6/TMC with 1% TMC.

3.3. Grafting copolymerization

Various parameters, mainly monomer and initiator concentrations, temperature, duration of reaction, and addition of crosslinker were found to influence the grafting polymerization of acrylamide. The effect of these variables was studied and summarized in **Table (6)**. The experiments were designed to change only one parameter each time while keeping the others constant. The grafting was elucidated by FTIR, TGA, SEM images and contact angle measurements.

- **Effect of initiator concentration**

The initiation of graft copolymerization was carried out using redox initiation system consists of potassium persulfate/sodium bisulfite at molar ratio

1:2. The effect of initiation system concentration on the grafting percent was studied and shown in **Fig. (7- a)**. It was observed that increasing the potassium persulfate concentration up to 20 Mm/L increases the grafting yield to 16.5± 0.56% due to the generation of more radical sites on fibers and increasing the growing chains. However, further increase in initiator concentration led to significant decrease in grafting rate. This could be attributed to the excess generation of free radicals terminating the growing chains **[45]**. The proposed mechanism of graft copolymerization can be explained as follow: The graft copolymerization-initiation (reaction of bisulfite and hydroxyl radicals with sulfate radical anions) that attack the nanofibrous mat, producing macroradicals **[46]**. Then the addition of acrylamide onto the fibers was attempted.

Table (6): Summary of various parameters that affected grafting reaction. Values are presented as mean ± S.D. (n=3).

Sample code	Parameters					Average grafting %
	Initiator Conc. mM/l	Monomer conc. Wt. %	Tem. ℃	Time Min	Crosslinker Wt. %	
A1	5	20	60	60	-	6 ± 0.46
A2	10					9 ± 0.72
A3	15					14.5 ± 0.66
A4	20					16.5 ± 0.56
A5	25					10 ± 0.62
B1	20	15	60	60	-	3.4 ± 0.82
A4		20				16.5 ± 0.56
B2		25				44 ± 2.19
B3		30				76 ± 2
B4		35				77 ± 1.32
C1	20	20	40	60	-	5 ± 1.14
C2			50			10 ± 1.76
A4			60			16.5 ± 0.56
C3			70			17 ± 0.44
C4			80			16 ± 1
D1	20	20	60	30	-	8.3 ± 1.15
A4				60		16.5 ± 0.56
D2				90		16.8 ± 0.61
D3				120		16.9 ± 0.61
D4				150		17 ± 0.5
E	20	25	60	60	1%	170 ± 25.17

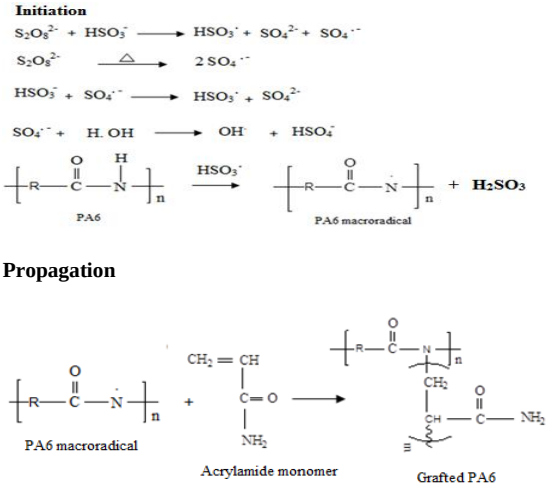

Scheme (1): The proposed reactions involved in the grafting process

- **Effect of monomer concentration**

It can be seen from **Fig. (7- b)** that at the lowest monomer concentration of (15 wt. %), the grafting ratio was only 3.4 ± 0.82 % indicating nearly no grafting reaction. However, with increasing the monomer concentration, the grafting ratio increased steadily and grafting percent of 76± 2 % was obtained at 30 wt.% as high monomer concentration resulted in increased availability for grafting reaction and production of more polymerization chains. Nevertheless, when the monomer concentration was increased, there was no appreciable effect on the grafting ratio, probably due to the greater tendency for homopolymerization and increased viscosity of the medium which hindered diffusion of radicals and monomer to the active sites on the fibrous mat **[47].**

- **Effect of temperature**

From **Fig. (7-c),** it is noticed that the grafting percentage was successively increasing with temperature up to 60 ℃ and then levelled off at 70 ℃, which could be attributed to the increase in both initiation and propagation rates. When the

temperature exceeded 70 ℃, grafting ratio decreased due to the increased termination rate **[47]**

- **Effect of reaction time**

Fig. (7- d) shows that the grafting percentage increased dramatically with the progression of the reaction time and then it levelled off after 1 hour. During the first hour of the reaction there was much more monomer than the free radicals therefore the propagation reaction is the dominant process. After that, the monomer was consumed and its concentration decreased compared to the free radicals and the reaction terminated **[47]**.

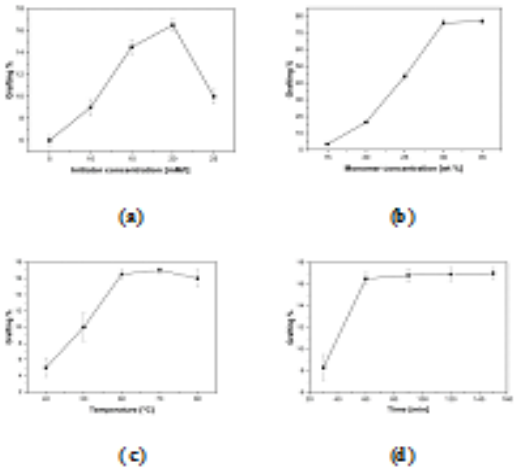

Figure (7): Effect of **(a)** initiator concentration, **(b)** monomer concentration, **(c)** temperature and **(d)** reaction time on grafting percentage. Data are presented as mean ± S.D. (n= 3)

- **Effect of crosslinker**

Cross-linked polyacrylamide hydrogel grafted layer was formed in the presence of the crosslinker (N, N methylene bis acrylamide) at 1% w/w ratio based on monomer weight. The added crosslinker is a polyfunctional molecule with four reactive sites with a structure of **CH_2=CHCONH– CH_2 – NHCOCH=CH_2** that can bridge the radicals on the growing polyacrylamide chains leading to the formation of a crosslinked network of polyacrylamide**[48]** and increasing the grafting ratio to as high as 170 ± 25.17 %.

- **FTIR Analysis**

Fig. (8) shows the ATR-FTIR spectroscopy results for ungrafted PA6/TMC, and polyacrylamide grafted PA6/TMC (44 %, and 76 % grafting ratio). It is noticed that ungrafted PA6/TMC showed absorption peaks at 3297 due to –NH stretching, 1636 corresponding to –C=O stretching and the combined absorption peak of both -NH and C-N at 1543.

The results for the polyacrylamide grafted PA6/TMC (PAM grafted PA6/TMC) show that the absorption peak at around 1536 for the combined absorption of -NH and C-N was weakened after grafting reaction and with increasing the grafting percent indicating the involvement of the –NH groups of PA6 in the grafting reaction **[47]**. At the same time, the emergence of the absorption peaks above 3700 assigned to –NH2 bonded to water –OH confirms the grafting of polyacrylamide to PA6/TMC nanofibrous mat.

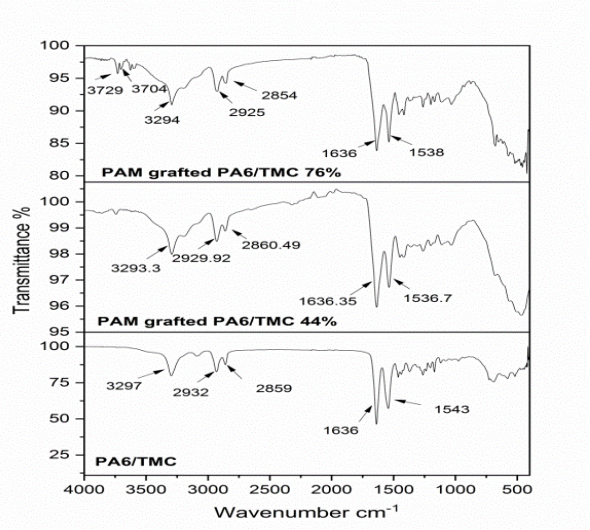

Figure (8): ATR-FTIR spectra of ungrafted PA6/TMC nanofibrous mat,polyacrylamide grafted PA6/TMC with 44% grafting percent, polyacrylamide grafted PA6/TMC with 76% grafting percent

- **Thermal gravimetric analysis (TGA)**

The effect of polyacrylamide grafting on the thermal stability of the PA6/TMC nanofibrous mat was investigated by TGA in the range of 50 – 600 ℃. TGA data presented in table 7 and **Fig. (9),** shows that ungrafted PA6/TMC nanofibers started degradation at 410℃ and reached maximum decomposition at 458 ℃ with 75% weight loss. The onset degradation temperature of polyacrylamide grafted PA6/TMC nanofibers was much lower than that of the ungrafted sample. 76% grafting ratio decreased the onset decomposition to 357.45 ℃ compared to 410 ℃ for the ungrafted sample. This could be attributed to the grafted polyacrylamide chains being more susceptible to break down detach from the hosting polymer backbone **[46, 47].**

The char residue for ungrafted PA6/TMC nanofibers was only 17.8% at 600 ℃ but reached 42% at the same temperature after grafting with polyacrylamide.

Table (7) TGA results for ungrafted PA6/TMC and polyacrylamide grafted PA6/TMC (76% grafting ratio)

Sample type	Decomposition temperature (℃)				
	T 10%	T 20%	T 30%	T 50%	T 75%
Ungrafted PA6/TMC	410	422	430	441.8	458
Grafted (76%) PA6/TMC	357.45	390.92	413	451.6	-

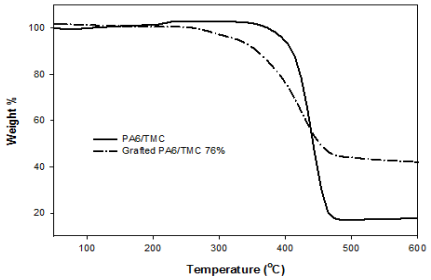

Figure (9): TGA curves for PA6/TMC nanofibrous mat and polyacrylamide grafted PA6/TMC (76% grafting ratio)

- **Morphology**

The surface of polyacrylamide grafted PA6/TMC nanofibrous mat was detected by SEM images and presented in **Fig. (10)**. The grafting polymerization reaction changed the morphology of the electrospun PA6/TMC nanofibrous mat. The surface of nanofibrous mat before grafting appeared with smooth and uniform fibers, while the surface of polyacrylamide grafted nanofibrous mat (76% grafting ratio) became rough and less uniform and the average fiber diameter increased from 78.5 ± 3.92 nm to 139 ± 28.36 nm due to the formation of graft layer on the surface of the fibers **[23]**.

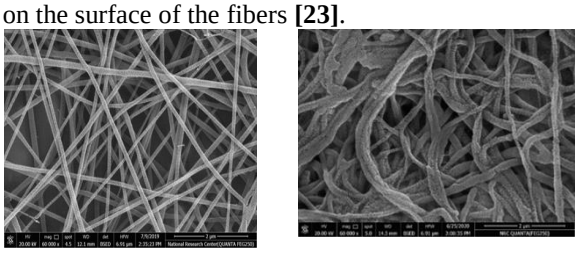

a **b**

Figure (10): SEM images of **(a)** PA6/TMC nanofibrous mat and **(b)** polyacrylamide grafted PA6/TMC nanofibrous mat (76% grafting ratio)

- **Contact angle measurements**

The contact angle is defined as the angle that a drop of liquid creates when it comes in contact with a solid surface. It quantitatively measures the wetting ability of a surface by a liquid, and the smaller the contact angles, the larger the wetting ability. Contact angle with a liquid ranging from [0 - 90°] indicates good wettability with this liquid but when a liquid creates contact angle between [90 - 180°] is considered not wetting liquid [**49]**. The water contact angle was used to investigating the effect of grafting on hydrophilicity and wettability of PA6/TMC nonofibrous mat surface **[50]**. The contact angle values for ungrafted and grafted nanofibrous mat are shown in **Fig. (11- A).** It was found that, the value of contact angle for ungrafted nanofibrous mat was zero, indicating excellent wetting and complete absorption of water drop by the surface due to its uniformity, smoothness and the presence of interfibers pores **[51]**. On the other hand, the contact angle for polyacrylamide grafted mat (76% grafting ratio) increased to 63.2 ± 3.46° as the grafting reaction disrupted the surface uniformity and increased its roughness as confirmed from SEM images.

- **Swelling behaviour**

Grafted polyacrylamide hydrogel layer to the nanofibrous mat can swell and retain a considerable amount of liquid in its network structure. In addition, the nanofibrous mat has a large surface area, and enhanced wettability and absorption capacity.

Therefore, the weight of swollen hydrogel sample was estimated, and the swelling ratio was calculated at several time points. The curve of swelling ratio variation with time for the crosslinked polyacrylamide grafted nanofibrous mat is presented in **Fig. (11- B)**.

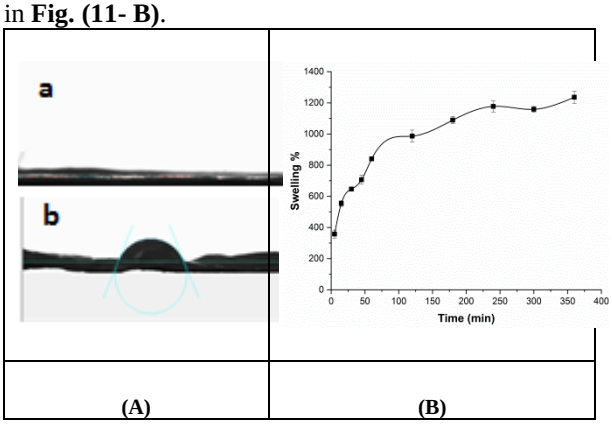

Figure (11): (A) Contact angle measurement of (a) ungrafted and (b) 67% polyacrylamide grafted PA6/TMC nanofibrous mat. (B) Swelling of crosslinked polyacrylamide grafted nanofibrous mat in PBS (pH 7.4) Values are presented as mean ± S.D. (n=3).

It can be noticed that, the swelling ratio significantly increased with time and a swelling ratio of 1236 ± 39.98 % was achieved in six hours **[19].**

3.4. Drug loading

Polyacrylamide hydrogel is a biocompatible material extensively applied for drug delivery due to its high swelling ability **[19, 52]**. Therefore, the efficiency of

the prepared crosslinked polyacrylamide grafted PA6/TMC nanofibrous mat as a drug vehicle was investigated by incorporating doxycycline hydrochloride into the grafted nanofibrous material through the swelling diffusion method as the grafted hydrogel layer can swell and retain the drug in its network structure **[19, 27]**. Furthermore, drug loading was carried out in drug solution at pH 4 and 6 to explore the best loading conditions.

- **Drug content**

Drug content within the grafted nanofibrous material was estimated experimentally by completely eluting the drug from the loaded sample in 30 ml of PBS (pH 7.4) for 24h and estimating drug mass released in the medium by UV spectrophotometer at λ_{max} 273 nm. The loading content was calculated according to equation **(3) [53]**

$$\text{Loading content\%} = (M_{drug} / M_{loaded\ sample}) \times 100 \quad (3)$$

Where **(M_{drug})** represents the total amount of drug liberated from the sample, and **($M_{loaded\ sample}$)** represents the mass of loaded sample. **Table (8)** summarizes the values of drug content obtained and the corresponding loading content ratio. It was found that the loaded drug increased by 31.5% from 76 ± 4.68 to 100 ± 11.98 mg/gm by increasing the pH of initial drug solution from 4 to 6. When the grafted material is soaked in a drug solution, water in which the drug is solubilized starts to diffuse into the polymeric network. Since the pH value has a remarkable influence on the swelling ratio of hydrogels thus, the loading content was mainly influenced by the absorption capacity of crosslinked polyacrylamide grafted fibers **[54]**. At pH 4 (relatively low) the amide groups (– $CONH_2$) remain unionized, resulting in collapsed network state. In contrast, with increasing the pH value to 6, the amide groups are partially ionized producing carboxylate anions (COO^-) which increase repulsion inside the gel network leading to enhance swelling of the polymeric chains **[48]**.

Table (8): Drug content incorporated into grafted nanofibrous mat at different loading conditions Values are presented as mean ± S.D. (n=3)

Sample type	Initial drug conc. mg/ml	pH	Drug content mg/gm	Loading content %
Grafted nanofibers	10	4	76 ± 4.68	7.6 ± 0.46
		6	100 ± 11.98	10 ± 1.19

- **In-vitro drug release studies**

The release behaviour of doxycycline hydrochloride from cross-linked polyacrylamide grafted PA6/TMC nanofibrous mat was studied in two different release media; PBS (pH 7.4) and acetate buffer (pH 5.5) as a function of time. The drug release profiles are shown in **Fig. (12-A),** and it can be observed that, the drug released fast in both release media, and initial burst release was noticed during the first two hours; about 58.54± 1.03 %, and 59.66 ± 0.91% of total drug content were eluted in PBS (pH 7.4) and acetate buffer (pH 5.5), respectively, in the first two hours. In addition, a maximum release of 94.56 ± 1 % was achieved from the grafted nanofibrous mat in PBS compared to approximately 89 ± 0.79 % in acetate buffer over duration for eight hours.

Furthermore, the drug release behavior from cross-linked polyacrylamide grafted PA6/TMC nanofibrous mat was studied in PBS (pH 7.4) as a function of drug content. It was observed from **Fig. (12-B)** that the content of loaded drug influenced the release behavior. The release profile of the low drug loading grafted nanofibrous mat in PBS (pH 7.4) showed a slower rate compared to the high drug loading material in the same release medium. For example, only 50.91 ± 0.91 % of the drug content was released from the low loading sample during the first two hours compared to 58.5 ± 1.03 % from the highly loaded sample in PBS. Similarly, a maximum cumulative release of 83.51 ± 1.26 % was achieved from low loading material while as high as 94.56 ± 1% cumulative release was achieved from high loading material within eight hours. These results were consistent with previous work **[55].**

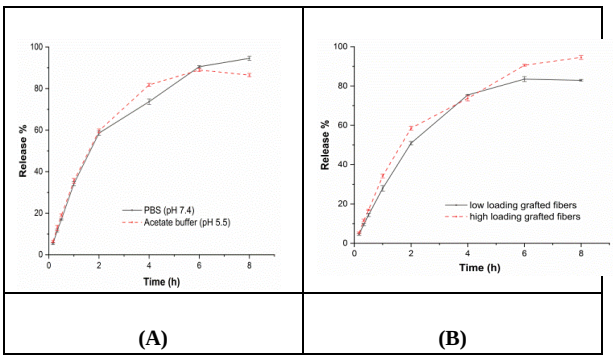

Figure (12). Drug release profile of Doxycycline hydrochloride from crosslinked polyacrylamide grafted PA6/TMC nanofibrous mat **(A)** in buffer solution with different pH (7.4, 5.5) and **(B)** with different drug loading in PBS (pH 7.4). Values are presented as mean ± S.D. (n=3)

3.5. Antimicrobial Evaluation

The antimicrobial efficacy of doxycycline hydrochloride loaded cross-linked polyacrylamide grafted nanofibrous mats was evaluated against *S. aureus* as an example of gram-positive bacteria, and *E. coli* as gram negative bacteria. Blank and free drug impregnated sterile susceptibility discs, and blank grafted nanofibrous mat were also applied as

controls. The antimicrobial activities of tested materials were studied by measuring the inhibition zones after 24 hours of incubation at 37 ℃ **[56]**.

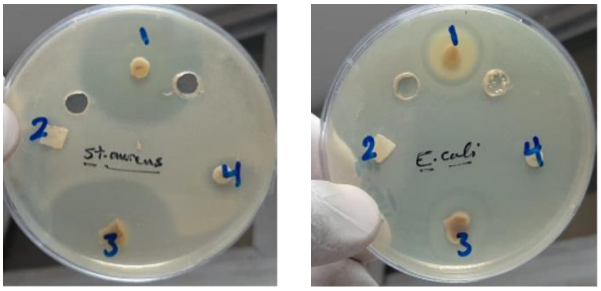

a **b**

Figure (13): Inhibition zones of **(1)** free drug, **(2)** blank grafted nanofibrous mat, **(3)** drug loaded grafted nanofibrous mat and **(4)** blank water against *S. aureus* **(a)**, and *E. coli* **(b)**

Clear inhibition zones were observed for loaded grafted nanofibrous mat samples against both types of bacteria as shown in **Fig. (13).** In contrast, blank grafted materials did not exhibit any antimicrobial inhibition. The diameters of inhibition zones were measured as 34 mm, and 22 mm against *S. aureus*, and *E. coli*, respectively. Furthermore, these inhibition zones were compared with the zones produced from sterile susceptibility discs impregnated with equivalent amount of free drug. which exhibited nearly similar inhibition zones of 36 mm, and 20 mm against *S.aureus*, and *E.coli* respectively indicating that loading process of the drug into grafted nanofibrous mat did not affect its efficacy and its antimicrobial activity **[57]**. The variation observed for inhibition zones diameters between the tested microorganisms is attributed to the high innate efficacy of doxycycline hydrochloride against gram-positive bacteria than gram-negative species **[58]**.

4. Conclusion

Polyacrylamide was grafted onto PA6/TMC nanocomposite fibrous mat through free radical polymerization using potassium persulfate and sodium hydrogen sulfite redox initiation system. Different parameters including (temperature, initiator and monomer concentration, and duration of reaction) were affected on the grafting polymerization reaction. In addition, methylene bis-acrylamide was good crosslinker for polyacrylamide hydrogel grafted to the nanofibers which was further assessed in drug loading and drug release of doxycycline hydrochloride. Crosslinked polyacrylamide grafted nanofibrous mat showed excellent absorption capacity and the drug released relatively fast in both PBS (pH 7.4), and acetate buffer pH (5.5). Also, the obtained results showed an effective antibacterial action against gram positive bacteria than gram negative species.

5. Conflicts of interest

There are no conflicts to declare.

6. References

[1] Yalcinkaya F., Yalcinkaya B. and Hruza J., Electrospun Polyamide-6 Nanofiber Hybrid Membranes for Wastewater Treatment., *Fibers and Polymers*, *20*(1), 93–99 (2019). https://doi.org/10.1007/s12221-019-8820-4

[2] Vasiljevic J, Colovic M., Jerman I., Simon B., Sest E., Golja B., Leskov M., Barbalini M., Malucelli G. and Bolka S., In situ prepared polyamide 6 / DOPO-derivative nanocomposite for melt-spinning of flame retardant textile filaments. *Polymer Degradation and Stability*, *166*, 50–59 (2019). https://doi.org/10.1016/j.polymdegradstab.2019.05.011

[3] Nguyen-Tran H, Hoang V, Do V, Chun D, Yum Y., *Effect of Multiwalled Carbon Nanotubes on the Mechanical Properties of Carbon Fiber-Reinforced* Polyamide 6/Polypropylene composites for light ewight automotive parts. Materials, 11, 429, (2018). https://doi.org/10.3390/ma11030429

[4] Nishiguti L., Erick S., Ribeiro G., & Ferreira G.. *Development of antistatic packaging of polyamide 6 / linear low - density polyethylene blends - based carbon black composites*. Polymer Bulletin, 7, 3389–3409 (2020).

[5] Winnacker M. Polyamides and their functionalization: recent concepts for their applications as biomaterials. *Biomaterials Science*,*5*,1230–1235,(2017). https://doi.org/10.1039/c7bm00160f

[6] Dantas de Oliveira A. and Augusto Gonçalves Beatrice C., Polymer Nanocomposites with Different Types of Nanofiller. *Nanocomposites - Recent Evolutions*. Chapter 6, 103 (2019). https://doi.org/10.5772/intechopen.81329

[7] Zhu T., Zhou C., Kabwe F, Wu Q. Q., Li C. and Zhang, J. Exfoliation of montmorillonite and related properties of clay/polymer nanocomposites. *Applied Clay Science*, ***169***, 48–66(2019). https://doi.org/10.1016/j.clay.2018.12.006

[8] Shah K. J, Mishra M., Shukla A. D., Imae T. and

Shah D. O., Controlling wettability and hydrophobicity of organoclays modified with quaternary ammonium surfactants. *Journal of Colloid and Interface Science, 407*, 493–499 (2013). https://doi.org/10.1016/j.jcis.2013.05.050

[9] Fu S., Sun Z., Huang P., Li Y. and Hu N. Some basic aspects of polymer nanocomposites : A critical review. *Nano Materials Science, 1*(1), 2–30(2019) https://doi.org/10.1016/j.nanoms.2019.02.006

[10] Rahmani M., Bidgoli S., & Rezayat S.. *Electrospun polymeric nanofibers for transdermal drug delivery*. Nanomed J, 42, 61-70, (2017) https://doi.org/ 10.22038/nmj.2017.21210.1224

[11] Ye K., Kuang H., You Z., Morsi Y., and Mo X. Electrospun Nanofibers for Tissue Engineering with Drug Loading and Release. *Pharmaceutics*. 11(4),182 (2019) doi: 10.3390/pharmaceutics11040182

[12] Oktay B., Demir S., and Kayaman-Apohan N., Immobilization of α -amylase onto poly (glycidyl methacrylate) grafted electrospun fibers by ATRP. *Materials Science and Engineering: C, 50*, 386–393 (2015). https://doi.org/10.1016/j.msec.2015.02.033

[13] Naragund V. S. and Panda P. K., Electrospun polyacrylonitrile nanofiber membranes for air filtration application. *International Journal of Environmental Science and Technology, published online October (2021)*. https://doi.org/10.1007/s13762-021-03705-4

[14] Liu X., Xu H., Zhang M. and Yu D. G., Electrospun medicated nanofibers for wound healing: Review. *Membranes*, *11*(10) 770. (2021). https://doi.org/10.3390/membranes11100770

[15] Luraghi A., Peri F. and Moroni L., Electrospinning for drug delivery applications : A review. *Journal of Controlled Release*, *334*, 463–484(2021). https://doi.org/10.1016/j.jconrel.2021.03.033

[16] Xue J., Wu T., Dai Y., and Xia Y., Electrospinning and electrospun nanofibers: Methods, materials, and applications. *Chemical Reviews*, *119*(8), 5298–5415 (2019). https://doi.org/10.1021/acs.chemrev.8b00593

[17] Zhao M., Yang Y., Yu H., Zhang X., Tian X., Fu S. and Zhang H., Improving the biofouling resistance of polyamide thin-film composite membrane via grafting polyacrylamide brush on the surface by in-situ atomic transfer radical polymerization. *Journal of Membrane Science, 629* (1–9):119283 (2021). DOI:10.1016/j.memsci.2021.119283

[18] Maji B., and Maiti S., Chemical modification of xanthan gum through graft copolymerization : Tailored properties and potential applications in drug delivery and wastewater treatment. *Carbohydrate Polymers*, *251*, 117095 (2021). https://doi.org/10.1016/j.carbpol.2020.117095

[19] Díaz -guerrero A, Castillo-miranda C, and Peraza-vázquez H., Modelling of acetaminophen release from hydroxyethylcellulose/ polyacrylamide hydroge*Materials Research Express* 8 (2021) 015310. https://doi.org/10.1088/2053-1591/abdc38.

[20] Lumbreras-aguayo A., Meléndez-ortiz H. I., Puente-urbina B., Alvarado-canché C., Ledezma A., Romero-garcía J. and Betancourt-galindo R., Poly (methacrylic acid) -modified medical cotton gauzes with antimicrobial and drug delivery properties for their use as wound dressings. *Carbohydrate Polymers, 205*, 203–210 (2019). https://doi.org/10.1016/j.carbpol.2018.10.015

[21] Richardson M, Kim J., Ho D., Snyder C, D'souza N., and Holmes G. Organofunctionalized Montmorillonite / Epoxy Nanocomposites : The Effect of Interlayer Cation Distribution on Mechanical Properties. *Polymer composites*, 32:67–78 (2011). https://doi.org/10.1002/pc

[22] Sobh R, Ekram B., and Mohamed W. Fabrication of Acrylic Modified Surface of Polyamide 6/CaO Electrospun Nanofibrous Membrane for Effective Dye Removal. *Egyptian Journal of Chemistry*. *63*(6), 2249–2260 (2020). https://doi.org/10.21608/ejchem.2019.19498.2187

[23] Ifuku S., Iwasaki M., Morimoto M. and Saimoto H., Graft polymerization of acrylic acid onto chitin nanofiber to improve dispersibility in basic water. *Carbohydrate Polymers*, *90*(1), 623–627 (2012). https://doi.org/10.1016/j.carbpol.2012.05.087

[24] Hong T., Ngo A., Do K. D. and Tran D. T., Surface modification of polyamide TFC membranes via redox-initiated graft polymerization of acrylic acid. *Journal of Applied Polymer Science, 45110*, 1–8 (2017). https://doi.org/10.1002/app.45110

[25] Gulsonbi M., Parthasarathy S., Raj K. B. and Jaisankar V. *Green synthesis , characterization and drug delivery applications of a novel silver /* carboxymethylcellulose – poly (acrylamide) hydrogel nanocomposite. *Ecotoxicology and Environmental Safety*, *134*, 421–426 (2016). https://doi.org/10.1016/j.ecoenv.2015.10.031

[26] Qiao Z., Tran L., Parks J., Zhao Y., Hai N., Zhong Y.and Ji H.-F., Highly stretchable gelatin-polyacrylamide hydrogel for potential transdermal drug release. *Nano Select*, 2, 107–115(2021). https://doi.org/10.1002/nano.202000087

[27] Qi X., Wei W., Li J., Liu Y., Hu X., Zhang J., Bi L. and Dong W., Fabrication and Characterization of a Novel Anticancer Drug Delivery System : Salecan / Poly (methacrylic acid) Semi-interpenetrating Polymer Network

Hydrogel. *ACS Biomaterials Science & Engineering*, 1, 1287−1299 (2015). https://doi.org/10.1021/acsbiomaterials.5b00346

[28] Kataria K., Gupta A., Rath G., Mathur R. B. and Dhakate S. R., In vivo wound healing performance of drug loaded electrospun composite nano fibers transdermal patch. *International Journal of Pharmaceutics*, *469*(1), 102–110 (2014). https://doi.org/10.1016/j.ijpharm.2014.04.047

[29] Sobh R. A., Nasr H. E., Moustafa A. B.,& Mohamed W. S.. *Tailoring of anticancer drugs loaded in MWCNT/Poly(MMA-co-HEMA) nanosphere composite by using in situ microemulsion polymerization*. Journal of pharmaceutical investigation,*49*(1),45–55 (2019). https://doi.org/10.1007/s40005-018-0390-8

[30] Menazea A. A., Ismail A. M., and Samy A., Novel Green Synthesis of Zinc Oxide Nanoparticles Using Orange Waste and Its Thermal and Antibacterial Activity. *Journal of Inorganic and Organometallic Polymers and Materials*, *0123456789*, 1–10 (2021). https://doi.org/10.1007/s10904-021-02074-2

[31] Haerdi-landerer M. C., Suter M. M., Steiner A., Wittenbrink M. M., Pickl A. and Gander B. A., In vitro cell compatibility and antibacterial activity of microencapsulated doxycycline designed for improved localized therapy of septic arthritis. *Journal of Antimicrobial Chemotherapy*, *61*(2), 332–340(2008). https://doi.org/10.1093/jac/dkm491

[32] Sarkar B., Megharaj M., Xi, Y., and Naidu R. Structural characterisation of Arquad ® 2HT-75 organobentonites: Surface charge characteristics and environmental application. *Journal of Hazardous Materials*, *195*, 155–161(2011). https://doi.org/10.1016/j.jhazmat.2011.08.016

[33] Singla P., Mehta R., and Upadhyay S. N., Clay Modification by the Use of Organic Cations, *Green and Sustainable Chemistry*, *2*(01), 21–25 (2012). https://doi.org/10.4236/gsc.2012.21004

[34] Jafarbeglou M., Abdouss M.,Shoushtari A. M. and Jafarbeglou M., Clay nanocomposites as engineered drug delivery systems. *RSC Advances*, *6*, 50002–50016 (2016). https://doi.org/10.1039/c6ra03942a

[35] Santos A., Viante M. F., Pochapski D. J., Downs A. J., and Almeida C. A. P., Enhanced removal of p-nitrophenol from aqueous media by montmorillonite clay modified with a cationic surfactant. *Journal of Hazardous Materials*, *355*, 136–144 (2018). https://doi.org/10.1016/j.jhazmat.2018.02.041

[36] Effenberger F., Schweizer M. and Mohamed W. S., Synthesis and characterization of some polyacrylate/montmorillonite nanocomposites by In Situ emulsion polymerization using redox initiation system. *Journal of Applied Polymer Science*, *112*(3), 1572–1578 (2009). https://doi.org/10.1002/app.29605

[37] Mit-Uppatham C., Nithitanakul M. and Supaphol P., Ultrafine electrospun polyamide-6 fibers: Effect of solution conditions on morphology and average fiber diameter. *Macromolecular Chemistry and Physics*, *205*(17), 2327–2338 (2004). https://doi.org/10.1002/macp.200400225

[38] Li L., Bellan L. M., Craighead H. G. and Frey M. W., Formation and properties of nylon-6 and nylon-6/montmorillonite composite nanofibers. *Polymer*, *47*(17), 6208–6217 (2006). https://doi.org/10.1016/j.polymer.2006.06.049

[39] Elsayed N. H., Alsharif M. A. and Mohamed W. S., Preparation and Characterization of Melt Spun Polypropylene/Montmorillonite Nanocomposite Fibre for Ibuprofen Drug Delivery Application, *Egyptian Journal of Chemistry*, *61*(2), 259–268 (2018). https://doi.org/10.21608/EJCHEM.2018.2949.1244

[40] Saeed K., and Park S. Y., Effect of Nanoclay on the Thermal , Mechanical , and Crystallization Behavior of Nanofiber Webs of Nylon-6. *Polymer composites*, 33, 192–195 (2012). https://doi.org/10.1002/pc

[41] Wu H., Krifa M. and Koo J. H., Flame retardant polyamide6/nanoclay/intumescent nanocomposite fibers through electrospinning. *Textile Research Journal*, *84*(10), 1106–1118 (2014). https://doi.org/10.1177/0040517513515314

[42] Wang L.,Yan Y.B., Yang Q. Q., Yu J. and Guo Z.X., Polyamide 66 / organoclay nanocomposite fibers prepared by electrospinning. *Journal of Materials Science*, 47(4):1702-1709 (2012).. https://doi.org/10.1007/s10853-011-5949-y

[43] Gabr M. H. and Uzawa K., Mechanical , thermal , and interfacial shear properties of polyamide / nanoclay nanocomposites : Study the effect of nanoclay on the micromechanism of fracture. *Journal of Thermoplastic Composite Materials*, 31(4)447–464(2018). https://doi.org/10.1177/0892705717705692

[44] Wang Y., Gao, J., Ma, Y., and Agarwal, U. S., Study on mechanical properties , thermal stability and crystallization behavior of PET / MMT nanocomposites. *Composites Part B: Engineering*,*37*,399–407(2006). https://doi.org/10.1016/j.compositesb.2006.02.014

[45] Makhlouf C., Marais S., and Roudesli S., Graft copolymerization of acrylic acid onto polyamide fibers. *Applied Surface Science*, *253*(12), 5521–5528(2007). https://doi.org/10.1016/j.apsusc.2006.12.086

[46] Zhao Q., Gu X., Zhang S., Dong M., Jiang P., and Hu Z. Surface modification of polyamide 66 fabric by microwave induced grafting with 2-hydroxyethyl methacrylate. *Surface and Coatings*

Technology, *240*, 197–203 (2014). https://doi.org/10.1016/j.surfcoat.2013.12.003

[47] Li X., Gu X., Zhang S., Li H., Feng Q., Sun J. and Zhao Q., Improving the fire performance of nylon 6,6 fabric by chemical grafting with acrylamide. *Industrial and Engineering Chemistry Research*, *52*(6) 2290–2296 (2013). https://doi.org/10.1021/ie302452e

[48] Singh B., Chauhan G. S., Kumar S., and Chauhan N., Synthesis, characterization and swelling responses of pH sensitive psyllium and polyacrylamide based hydrogels for the use in drug delivery(I). *Carbohydrate Polymers*. *67(2)*, 190–200(2007). https://doi.org/10.1016/j.carbpol.2006.05.006

[49] Kurusu R. S. and Demarquette N. R., Surface modification to control the water wettability of electrospun mats. *International Materials Reviews*, 64,(5),249–287(2019). https://doi.org/10.1080/09506608.2018.1484577

[50] Park M. J., Gonzales R. R., Abdel-Wahab A., Phuntsho S. and Shon H. K., Hydrophilic polyvinyl alcohol coating on hydrophobic electrospun nanofiber membrane for high performance thin film composite forward osmosis membrane. *Desalination*, *426*, 50–59. (2018). https://doi.org/10.1016/j.desal.2017.10.042

[51] Hekmati A. H., Khenoussi N. and Nouali H., Effect of nanofiber diameter on water absorption properties and pore size of polyamide-6 electrospun nanoweb. *Textile Research Journal*, 84(19) 2045–2055 (2014). https://doi.org/10.1177/0040517514532160

[52] Birajdar, R. P., Patil, S. B., Alange, V. V, & Raghavendra, V.. Electro-responsive polyacrylamide-grafted-gum ghatti copolymer for transdermal drug delivery application. *Journal of Macromolecular Science, Part A*, *56*(4), 306–315,(2019). https://doi.org/10.1080/10601325.2019.1574539

[53] Carissimi G., Montalbán M. G., Víllora G. and Barth A., Direct quantification of drug loading content in polymeric nanoparticles by infrared spectroscopy. *Pharmaceutics*, *12*(10), 1–15, (2020). https://doi.org/10.3390/pharmaceutics12100912

[54] Ismail O. and Kocabay Ö. G., Absorption and adsorption studies of polyacrylamide / sodium alginate hydrogels. *Colloid and Polymer Science*, 299, 783–796 (2021). https://doi.org/10.1007/s00396-020-04796-0

[55] Sabbagh F., and Muhamad I. Acrylamide-based hydrogel drug delivery systems : Release of Acyclovir from MgO nanocomposite hydrogel, *Journal of the Taiwan Institute of Chemical Engineers*, *72*, 182–193 (2017). https://doi.org/10.1016/j.jtice.2016.11.032

[56] Chen H., Xing X., Tan H., Jia Y., Zhou T., Chen Y., Ling Z. and Hu X., Covalently antibacterial alginate-chitosan hydrogel dressing integrated gelatin microspheres containing tetracycline hydrochloride for wound healing. *Materials Science & Engineering C*, *70*, 287–295 (2017).. https://doi.org/10.1016/j.msec.2016.08.086

[57] Misra R. and Sahoo S. K., Antibacterial activity of doxycycline-loaded nanoparticles. *Methods in Enzymology*, 509, 61-85 (2012). https://doi.org/10.1016/B978-0-12-391858-1.00004-6

[58] Hamilton A. R., Roberts M., Hutcheon G. A. and Gaskell E. E., Formulation and antibacterial properties of clay mineral-tetracycline and -doxycycline composites. *Applied Clay Science*, *179*,105148(2019). https://doi.org/10.1016/j.clay.2019.105148